In-Plane Uniaxial Strain in Black Phosphorus Enables the Identification of Crystalline Orientation

Shuqing Zhang, Nannan Mao, Juanxia Wu, Lianming Tong, Jin Zhang,* and Zhirong Liu**

Identification of the crystalline axis of anisotropic black phosphorus (BP) is important for investigating its physical properties, as well as for optical and electronic applications. Herein, it is showed that by applying in-plane uniaxial strain and measuring the changes of the Raman shifts, the crystalline axis of BP can be reliably determined. The strain effects on the Raman shifts are angle-dependent, and they can be expressed as a combination of the Raman responses under zigzag and armchair strain. Differing from previous polarized optical spectroscopic methods where the Raman intensity is analyzed, the proposed method uses the Raman frequency shift, which is less affected by laser polarization, excitation wavelength, the sample thickness, and the substrate. The effective strain applied on BP from the stretched substrate is estimated, and the results show that only 20 to 40% of the strain can be effectively transferred to BP flakes from a polyethylene terephthalate substrate. Our method provides not only an effective and robust approach to identify the crystalline orientation of layered BP, but it is also a model to extract additional information in strain-related studies. It can also be extended to other 2D anisotropic materials.

1. Introduction

Black phosphorus (BP) is the most stable allotrope of crystalline phosphorus, and it is black and flaky like graphite.[1,2] Few-layer BP has many attractive features. For example, its bandgap is thickness dependent and can be tuned from 0.3 eV to around 2 eV.[3,4] The charge carrier mobility may exceed 1000 $cm^2V^{-1}s^{-1}$ at room temperature and even be tens of thousands at lower temperature.[5,6] Therefore, it has attracted tremendous interest since 2014.[7–9] Differing from isotropic 2D materials such as graphene and some transition metal dichalcogenides, BP is anisotropic with an orthorhombic structure. Its mechanical behavior,[10] electrical mobility,[11,12] optical absorption,[11,13] and thermoelectric[14] properties all depends on the crystalline orientation. To take advantage of the desirable anisotropic properties of BP and other anisotropic 2D materials, a nondestructive, effective, and applicable characterization tool to identify the crystalline orientation is urgently required.

Raman spectroscopy is a fast and nondestructive characterization method. The positions, intensities, and shapes of the bands in Raman spectroscopy contain amounts of information about the atomic structure, existing forms, defects, electronic and phonon properties of the samples, making it a necessary and standardized technique in the study of 2D materials.[15–17] The three usual characteristic Raman bands of BP are located at around 360, 440, and 470 cm^{-1} (**Figure 1**c), which are attributed to the A_g^1, B_{2g}, and A_g^2 modes, respectively. Based on the conventional selection rules of orthorhombic system, the intensity distributions from

S. Zhang, N. Mao, Dr. J. Wu, Prof. L. Tong, Prof. J. Zhang, Prof. Z. Liu
Center for Nanochemistry
College of Chemistry and Molecular Engineering
Peking University
Beijing 100871, P. R. China
E-mail: tonglm@pku.edu.cn; jinzhang@pku.edu.cn; liuzhirong@pku.edu.cn

S. Zhang, Prof. J. Zhang, Prof. Z. Liu
Academy for Advanced Interdisciplinary Studies
Peking University
Beijing 100871, P. R. China

DOI: 10.1002/smll.201700466

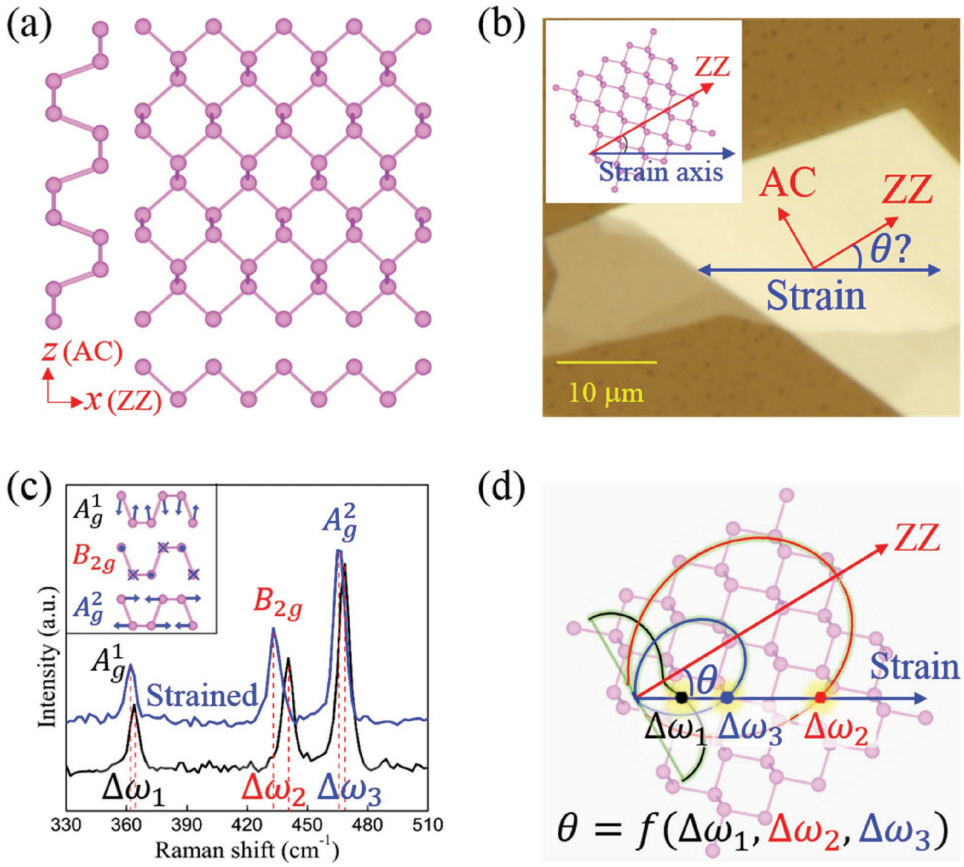

Figure 1. Determination of the crystalline orientation of BP from the shift patterns of the Raman bands under uniaxial strain. a) Geometrical structure of monolayer BP. The *x* and *z* axes are along the ZZ and AC directions, respectively, following the conventional notation in bulk BP. b) Optical image of a BP flake, the angle θ between the uniaxial strain and the ZZ direction is indicated. c) The corresponding Raman spectra of the strained (blue band) and unstrained (black band) BP flake in panel (b) under backscattering configurations. The inset shows the atomic displacements for the three characteristic Raman modes. d) Changes of the Raman shifts ($\Delta\omega_1$, $\Delta\omega_2$, $\Delta\omega_3$) under strain with different dependences on θ, and θ can be back-calculated from the measured pattern of ($\Delta\omega_1$, $\Delta\omega_2$, $\Delta\omega_3$).

Raman tensors are angle-resolved, so polarized Raman spectroscopy became an important tool for identifying the crystalline orientation of BP layers in the earlier studies.[18–20] However, it has been shown that the excitation wavelength and sample thickness both play important roles in the angle-dependent Raman intensity of BP crystals,[13,21,22] which complicates orientation identification by the polarized Raman method because complex intrinsic electron–photon and electron–phonon interactions have to be taken into account.[13] The polarized Raman method is only feasible with specific experimental settings and well-optimized conditions.[13,18,21,22] Angle-resolved infrared spectroscopy and direct-current conductivity have also been proposed for identifying the crystalline orientation of BP,[11,13] but the complex microabsorption setup and micro-nanofabrication strongly restrict their application. Here, rather than the peak intensity, we focus on another important factor: the Raman shift, which is mainly determined by the overall crystal structure and the bond lengths and angles, rather than by optical effects or interference effects from the excitation laser energy and the thickness of the BP flakes.[7,23–25] We will show that the changes of Raman shift under in-plane uniaxial strain are angle-dependent, and it can be used to reliably determine the crystalline orientation of BP samples.

The main idea is shown in Figure 1. The structure of monolayer BP is highly anisotropic (Figure 1a; Figure S1, Supporting Information), forming a strongly puckered honeycomb lattice with troughs running in a zigzag (ZZ) direction. Under in-plane uniaxial strain (with the orientation angle denoted as θ in Figure 1b), the frequencies of the three characteristic Raman modes clearly change compared with the unstrained case (Figure 1c). The frequency changes versus strain are angular dependent (solid curves in Figure 1d). By comprehensively considering the shift patterns of the three bands under a single strain (instead of the shift amplitude of one band because the actual strain in 2D system is often overestimated[24,26,27]), the strain angle θ and the crystalline orientation can be readily determined.

2. Results and Discussion

2.1. Model of Orientation-Dependent Raman Frequency Shifts versus Strain

Strain is a second-order tensor, and it can be written as a symmetric matrix in 2D system:

$$\boldsymbol{\varepsilon} = \begin{bmatrix} \varepsilon_{xx} & \varepsilon_{xz} \\ \varepsilon_{xz} & \varepsilon_{zz} \end{bmatrix} \tag{1}$$

where ε_{xx} and ε_{zz} are the uniaxial strain along the x and z axes, respectively, and ε_{xz} is the shear strain component. For uniaxial strain ε along any specified direction with angle θ, it can be expressed by a rotation transformation as:

$$\begin{aligned} \boldsymbol{\varepsilon}(\theta) &= \begin{bmatrix} \varepsilon_{xx} & \varepsilon_{xz} \\ \varepsilon_{xz} & \varepsilon_{zz} \end{bmatrix} = \boldsymbol{R}^T \begin{bmatrix} \varepsilon & 0 \\ 0 & 0 \end{bmatrix} \boldsymbol{R} \\ &= \begin{bmatrix} \varepsilon\cos^2\theta & -\varepsilon\sin\theta\cos\theta \\ -\varepsilon\sin\theta\cos\theta & \varepsilon\sin^2\theta \end{bmatrix} \end{aligned} \tag{2}$$

where $\boldsymbol{R}$ is the 2D rotation matrix for counterclockwise rotation through angle θ:

$$\boldsymbol{R} = \begin{bmatrix} \cos\theta & -\sin\theta \\ \sin\theta & \cos\theta \end{bmatrix} \tag{3}$$

When the applied strain is small, the phonon frequency linearly changes with strain,[28] and for nondegenerate modes, such as those in BP, it is:

$$\begin{aligned} \omega(\varepsilon,\theta) &= \omega_0 + k_x\varepsilon_{xx} + k_z\varepsilon_{zz} + 2k_\gamma\varepsilon_{xz} \\ &= \omega_0 + \left(k_x\cos^2\theta + k_z\sin^2\theta - 2k_\gamma\sin\theta\cos\theta\right)\varepsilon \end{aligned} \tag{4}$$

where k_x and k_z are the change rates of the frequencies versus strain along the ZZ and armchair (AC) directions, respectively, and k_γ is the rate under shear strain. Owing to the mirror reflection symmetry (perpendicular to the xz plane) of the orthorhombic structure, the frequency remains invariant under opposite shear strain [$\omega(\varepsilon_{xz},\theta) = \omega(-\varepsilon_{xz},\theta)$], so the contribution of shear strain to the frequency change is zero, i.e.

$$k_\gamma = 0 \tag{5}$$

Therefore, the frequency under uniaxial strain with directional angle θ becomes:

$$\omega(\varepsilon,\theta) = \omega_0 + \left(k_x\cos^2\theta + k_z\sin^2\theta\right)\varepsilon \tag{6}$$

Hence, the change rate of the frequency versus strain is angle-dependent:

$$k = \frac{\partial\omega}{\partial\varepsilon} = k_x\cos^2\theta + k_z\sin^2\theta \tag{7}$$

For monolayer BP, the Raman shifts of the A_g^1, B_{2g}, and A_g^2 modes under uniaxial strains along the ZZ and AC directions were calculated by density functional theory (DFT) (see Section 4 and the Supporting Information for details) and the results are summarized in **Figure 2**a–c. The frequencies of other optical phonons at the center of the Brillouin zone of monolayer BP are shown in Figure S4 in the Supporting Information. It can be seen that the change rates are different for the three modes. For the A_g^1 mode, the change under AC strain is larger than that under ZZ strain. In contrast, for the B_{2g} and A_g^2 modes, the Raman shifts change very little with AC strain, but show much larger shifts with ZZ strain. These features can be explained by the changes of the geometric parameters for the two typical directions.[24,25] As shown in the inset of Figure 1c, the atomic displacements of the modes mainly originate from relative vibration of the atoms within the layer, which are not sensitive to interlayer coupling. As a result, both calculations and experiments have shown that the Raman shifts of few-layer BP are almost unchanged for different flakes with distinct thicknesses.[7,23,24]

According to Equation (7), the change rates at any angle θ can be derived from the frequency responses along the ZZ direction (k_x) and AC directions (k_z). In Figure 2d–f, the results using Equation (7) are shown as solid lines using k_x and k_z determined from Figure 2a–c, and they are compared with the values obtained by direct DFT calculations at each θ (scattering point). The agreement is excellent, supporting the validity of Equation (7). In the case of $\theta = 30°$, the DFT calculated change rates are –1.91, –6.66, –3.34 cm^{-1}/% strain (Figure 2g–i) and the results from Equation (7) are –1.83, –6.92, and –3.35 cm^{-1}/% strain for the A_g^1, B_{2g}, and A_g^2 modes, respectively. The results of other optical phonons, such as the B_{1g}, B_{3g}, and A_u modes, are shown in Figures S4 and S5 in the Supporting Information.

2.2. Determination of the Crystalline Orientation of BP by the Change Rates of the Raman Shifts

From Equation (7), the change rates of the three Raman modes are θ dependent:

$$\begin{cases} k_1\left(A_g^1\right) = k_{1x}\cos^2\theta + k_{1z}\sin^2\theta \\ k_2\left(B_{2g}\right) = k_{2x}\cos^2\theta + k_{2z}\sin^2\theta \\ k_3\left(A_g^2\right) = k_{3x}\cos^2\theta + k_{3z}\sin^2\theta \end{cases} \tag{8}$$

where the subscripts 1, 2, and 3 denote A_g^1, B_{2g}, and A_g^2 modes, respectively. To facilitate the determination, we rewrite the change rates as three-component vectors, i.e.,

$$\vec{k} = \begin{pmatrix} k_1 \\ k_2 \\ k_3 \end{pmatrix} \vec{A} = \begin{pmatrix} k_{1x} \\ k_{2x} \\ k_{3x} \end{pmatrix} \vec{B} = \begin{pmatrix} k_{1z} \\ k_{2z} \\ k_{3z} \end{pmatrix} \tag{9}$$

The components of $\vec{A}$ and $\vec{B}$ are given in Figure 2a–c. Any three-component vector $\vec{k}$ can be written as a combination of $\vec{A}$, $\vec{B}$, and $\vec{A}\times\vec{B}$ as:

$$\vec{k} = \vec{A}a + \vec{B}b + \vec{A}\times\vec{B}c \tag{10}$$

or in matrix form as:

$$\begin{bmatrix} k_1 \\ k_2 \\ k_3 \end{bmatrix} = \left[\vec{A}, \vec{B}, \vec{A}\times\vec{B}\right] \begin{bmatrix} a \\ b \\ c \end{bmatrix} \tag{11}$$

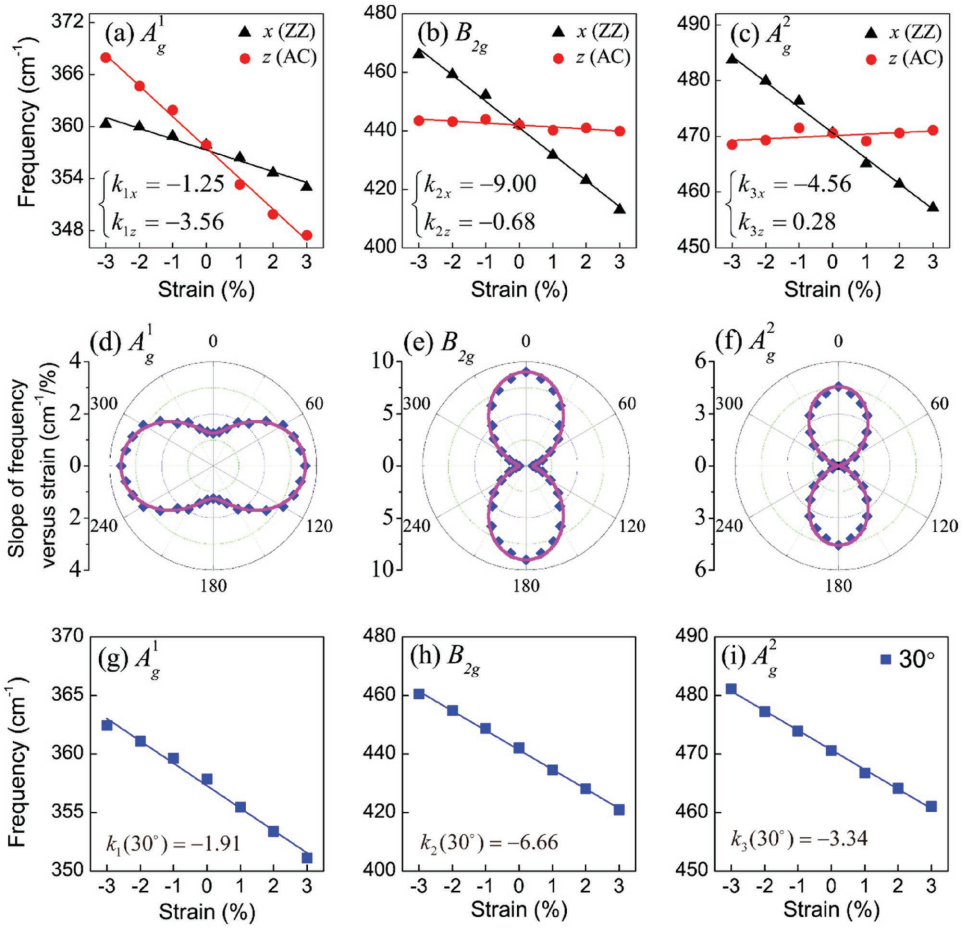

Figure 2. Change of the Raman shifts under uniaxial strain. a–c) Raman shifts versus uniaxial strain along *x* (ZZ) direction (black triangle) and *z* (AC) direction (red dot) of A_g^1, B_{2g}, and A_g^2 modes of monolayer BP. k_x and k_z (cm^{-1}/% strain) are the change rates of the frequency under these two typical directions. d–f) The corresponding θ-dependent change. The solid curves were calculated with Equation (7) with the k_x and k_z values determined in panels (a)–(c), and the scattering points were obtained with direct DFT calculations at each θ. g–i) Change rates of the Raman shifts under strain in the 30° case.

where a, b, and c are the combination coefficients. For given in Equation (8), $a = \cos^2\theta$, $b = \sin^2\theta$, and $c = 0$, which are functions of θ. The relationships indicate that, in theory, a and b are not less than zero. The measured quantities are the change rates of the Raman shifts ($\vec{k}$) in experiments. With Equation (11), it is straightforward to calculate a and b from the measured $\vec{k}$:

$$\begin{cases} a = 0.0129k_1 - 0.088k_2 - 0.0491k_3 \\ b = -0.2785k_1 + 0.0104k_2 + 0.0557k_3 \end{cases} \quad (12)$$

If the longitudinal strain is along the direction close to the *x* (0°) or *z* (90°) axis in the experiments, the a and b values calculated by the experimental rates may be less than zero, and we make additional definitions for such cases. A normalization processing is performed to balance the errors from the absolute measurements, as well as the mismatch between the strain applied on the substrate and the actual strain in the BP sample. The estimation of θ is:

$$\theta = \begin{cases} 0^\circ & (\text{if } b < 0) \\ 90^\circ & (\text{if } a < 0) \\ \arccos\sqrt{\dfrac{a}{a+b}} & (\text{if } a > 0 \text{ and } b > 0) \end{cases} \quad (13)$$

Here, we determine θ from the changes of all three modes, not only from one mode. This effectively reduces the error caused by experimental uncertainty, which will be demonstrated below.

To test the validity of the proposed method in detecting the BP orientation, we performed Raman experiments on a series of BP samples under different uniaxial strain. BP flakes of different thicknesses were mechanically exfoliated from bulk BP crystals onto flexible polyethylene terephthalate (PET) substrates. Optical images of the BP flakes are shown in **Figure 3**a–c. The sample thickness was determined by optical contrast method, and the fitted function of the sample thickness and optical contrast is shown in Figure S6 in the Supporting Information. According to the function, the thicknesses of the BP flakes in Figure 3a–c are 6.7, 14.5, and 9.8 nm, respectively. By stretching the substrates in a certain direction (the blue arrows in Figure 3a–c), uniaxial strain was controllably and uniformly introduced into the BP samples. In this study, uniaxial strain was applied along three directions: θ = 0° (ZZ), θ = 30°, and θ = 90° (AC). Angle-dependent polarized Raman spectroscopy was performed before applying strain to directly determine the crystalline orientation of the BP flakes in the experiments

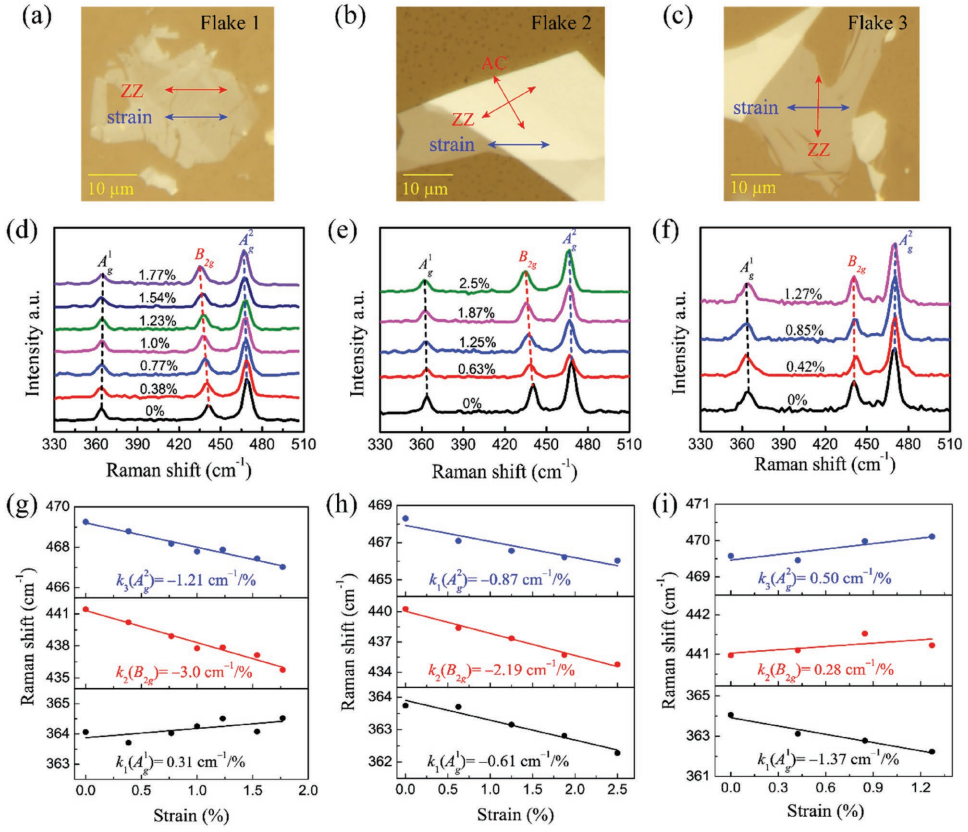

Figure 3. Determination of the BP orientation from the change of the Raman shifts under a uniaxial strain. a–c) Optical images of exfoliated BP flakes on the PET substrate. The uniaxial strain was applied at different angles: a) $\theta = 0°$, b) $\theta = 30°$, and c) $\theta = 90°$. d–f) Raman spectra of BP as the applied strain is gradually increased for the corresponding samples in panels (a)–(c) under 514.5 nm excitation. g–i) The corresponding fitted Raman shifts as a function of applied strain for the three BP flakes.

(more detail is given in Figure S7 of the Supporting Information). The Raman measurement results are summarized in Figure 3d–i. It is clear that the Raman peak positions change with applied strain (Figure 3d–f). The fitted frequencies as a function of strain are plotted in Figure 3g–i, and the obtained change rates k_1, k_2, and k_3, as well as the resulting a, b, and θ values from Equations (12) and (13), are listed in **Table 1**. The θ values determined from the proposed method are 0°, 33.3°, and 90° for the three samples, which agree well with the direct measurements (0°, 30°, and 90°).

We further tested the proposed method using reported experimental data of the Raman shifts under different strains. The sets of change rates (k_1, k_2,k_3) in **Table 2** were extracted from the literature.[24,25] The results for samples 4–6 (BP on PET) were obtained by 532 nm laser excitation, and they are hereafter referred to as spread BP@PET. The results for samples 7 and 8 were obtained under 488 nm laser excitation and the ultrathin BP was sandwiched by a top polymethyl methacrylate (PMMA) layer and a bottom PET substrate, and they are hereafter referred to as sandwiched PMMA@BP@PET. The thicknesses of the BP samples were within 50 nm for stretching. Samples 9, 10, 9^{β}, and 10^{β} are samples simulated by Li et al.,[25] where the Poisson's ratio of PET (0.33) was used for 9^{β} and 10^{β}. The θ values determined from the (k_1, k_2,k_3) data with our proposed method are in good agreement with the reported values, with the average discrepancy being as low as 4.1°. This further confirms the validity of the proposed method, which does not depend on the excitation wavelength, sample thickness, and substrate.

Table 1. Experimental determination of the BP orientation with the proposed method using the change rates (k_1,k_2,k_3) (in units of cm^{-1}/% strain) of the Raman shifts under uniaxial strain.

Sample #	$k_1(A_g^1)$	$k_2(B_{2g})$	$k_3(A_g^2)$	a	b	Angle θ [°]	
						Direct measurement[a)]	Proposed method[b)]
1	0.31	−3.0	−1.21	0.33	−0.18	0	0
2	−0.61	−2.19	−0.87	0.23	0.10	30	33.3
3	−1.37	0.28	0.5	−0.07	0.41	90	90

[a)]Determined by angle-dependent polarized Raman spectroscopy; [b)]Determined with the proposed Equations (12) and (13) by measuring the Raman shifts under strain.

Table 2. Determination of the BP orientation based on the reported change rates (k_1, k_2, k_3) (in units of cm^{-1}/% strain). α = The data were fitted according to the data in the references. β = The values were simulated with a Poisson's ratio of 0.33.

	Sample #	$k_1(A_g^1)$	$k_2(B_{2g})$	$k_3(A_g^2)$	a	b	Angle θ [°]	
							Refs.	Proposed method[a]
Expt.[24]	4	−1.3	-0.25^{α}	0.25^{α}	−0.007	0.373	75	90
	5	-0.31^{α}	−2.3	−1.1	0.253	0.001	10	3.62
	6	−1.1	−1.4	−0.5	0.134	0.264	56	54.6
Expt.[25]	7	−0.52	−10.92	−4.32	1.17	−0.21	0	0
	8	−3.81	−1.85	−0.03	0.115	1.04	90	71.6
Sim.[25]	9	0.19	−9.27	−4.06	1.02	−0.376	0	0
	9^{β}	1.12	−9.11	−4.1	1.018	−0.636	0	0
	10	−2.35	−0.7	0.52	0.006	0.680	90	84.8
	10^{β}	−2.21	2.16	2.01	−0.317	0.750	90	90

[a]Determined with the proposed Equations (12) and (13) from reported (k_1, k_2, k_3).

The proposed method is constructed based on the overall relative changes of three characteristic Raman modes rather than one absolute value, which is conductive to better accuracy under experimental uncertainties. The data in Tables 1 and 2 show that the absolute values of the change rates obtained by the spread BP@PET experiments (samples 1–6) are generally smaller than those obtained by the sandwiched PMMA@BP@PET experiments and the simulated results (samples 7–10). The most notable case is the Raman shift rates of the B_{2g} mode: the absolute rates for samples 7 and 8 obtained by sandwiched stacking are more than three times higher than those obtained for samples 1 and 3 with a spread structure even when the strain was applied in the same direction. Therefore, the criterion for identifying the orientation by the absolute change of one particular vibrational mode may be not suitable for different experimental configurations.[24,25] Our proposed method is able to compensate for the error caused by absolute measurements under different conditions.

2.3. Calculation of the Effective Strain Applied to BP

In practice, strain is applied directly on the substrate and then transfers to the supported 2D sheet such as BP. Strictly speaking, what is measured in experiments is the strain in the substrate, not that of the 2D sheet. Owing to the difference of the elastic constants (including Poisson's ratio) between the substrate and the 2D sheet and the weak interaction between them, slippage likely occurs at the interface between the 2D sheet and the substrate during stretching, leading to the efficiency of the applied strain and overestimation of the strain in the 2D sheet material. As a result, deviation of the measured physical properties would be observed.[24,25,28] Therefore, estimation of the effective strain is important, but it remains difficult. Based on the above results, here we develop a scheme to estimate the effective strain in a 2D sheet.

In an ideal situation, the applied efficiency of the strain can be estimated from any Raman mode of the BP flakes as the ratio of the experimental to calculated change rates under uniaxial strain:

$$\eta_i = \frac{k_i(\text{Expt.})}{k_i(\text{Calc.})}, \quad i = 1,2,3 \tag{14}$$

where k_i(Expt.) are measured values in experiments and k_i(Calc.) are the back-calculated values from Equation (8) using a θ value determined from k_i(Expt.), as explained in Section 2.2. In practice, data uncertainty is unavoidable, so we calculate the strain efficiency as the weighted average of η_i

$$\overline{\eta} = \frac{\sum_{i=1}^{3} \eta_i \left| k_i(\text{Calc.}) \right|}{\sum_{i=1}^{3} \left| k_i(\text{Calc.}) \right|} \tag{15}$$

The approach was applied to analyze different samples, and the results are summarized in **Table 3**. For the widely used spread BP@PET strain transfer setup, only 20– 40% of strain is effectively transferred from PET substrates to the BP flakes. It should be noted that mismatch does not influence determination of the crystalline orientation of BP in our proposed method because the influence of mismatch on a and b cancels in Equation (13). For the improved sandwiched PMMA@BP@PET experimental assembly, the strain can be considered to be completely transferred to the BP samples. In Table 3, almost all of the absolute rates in calculation are larger than, or at best close to the experimental measurements, except for the B_{2g} mode in the sandwiched system (samples 7 and 8). For the B_{2g} mode, atomic displacement is mainly along the ZZ direction (see Figure 1c), which slightly changes when strain is applied along the AC direction in theoretical calculations,[24,25,29] but the experimental value (–1.85) is three times larger than the calculated value (–0.68) for sample 8. The same discrepancy is also observed in the literature,[25] and this is mainly responsible for the mismatch angle of sample 8 in Table 2 and the unusual 124% strain efficiency in Table 3.

2.4. Simplified Model for Determination of θ

As shown in Section 2.2, θ of BP samples can be determined from the change rates (k_1, k_2, k_3) of the three characteristic

Table 3. Experimental (Expt.) and calculated (Calc.) Raman shift rates ($\partial\omega/\partial\varepsilon$, cm^{-1}/% strain) of the three characteristic Raman modes and the efficiency of the applied strain in experiments.

Sample #	θ [°]		$k_1(A_g^1)$	$k_2(B_{2g})$	$k_3(A_g^2)$	Strain efficiency[a]
1	0°	Expt.	0.31	−3.0	−1.21	26.33%
		Calc.	−1.25	−9.0	−4.56	
2	30°	Expt.	−0.61	−2.2	−0.87	30.4%
		Calc.	−1.83	−6.92	−3.35	
3	90°	Expt.	−1.37	0.28	0.5	35.2%
		Calc.	−3.56	−0.68	0.28	
4	75°	Expt.[24]	−1.3	−0.25	0.25	27.7%
		Calc.	−3.4	−1.24	−0.044	
5	10°	Expt.[24]	−0.31	−2.3	−1.1	27.5%
		Calc.	−1.32	−8.75	−4.41	
6	56°	Expt.[24]	−1.1	−1.4	−0.5	40.8%
		Calc.	−2.84	−3.28	−1.23	
7	0°	Expt.[25]	−0.52	−10.9	−4.32	106%
		Calc.	−1.25	−9.0	−4.56	
8	90°	Expt.[25]	−3.81	−1.85	−0.03	124%
		Calc.	−3.56	−0.68	0.28	

[a]Determined with Equation (15).

Raman shifts according to Equations (12) and (13), where (k_1, k_2, k_3) are fitted from a series of data points with different strain amplitude. As discussed in Sections 2.2 and 2.3, the strain may not be effectively applied to BP in experiments. However, our method is not directly related to the absolute applied strain, and it only depends on the relative changes of the three characteristic Raman shifts. Therefore, (k_1, k_2, k_3) can be replaced by the changes of the Raman shifts ($\Delta\omega_1$, $\Delta\omega_2$, $\Delta\omega_3$) under two different strain amplitudes, regardless of the actual values. Thus, Equation (12) can be simplified as:

$$\begin{cases} a = 0.0129\Delta\omega_1 - 0.088\Delta\omega_2 - 0.0491\Delta\omega_3 \\ b = -0.2785\Delta\omega_1 + 0.0104\Delta\omega_2 + 0.0557\Delta\omega_3 \end{cases} \quad (16)$$

Taking sample 2 as an example, three groups of points under distinct strain in Figure 3h were selected, and the various frequency changes ($\Delta\omega_1, \Delta\omega_2, \Delta\omega_3$) are analyzed in **Table 4**. Substituting the changes ($\Delta\omega_1$, $\Delta\omega_2$, $\Delta\omega_3$) into Equations (13) and (16), the θ values were also determined. The accuracy of θ in this simplified scheme is acceptable. Therefore, the advantage of our method is clear: the angle between the strain and the lattice is only related to the frequency changes under a distinct strain, and it does not matter whether the initial state is unstrained or strained. This provides a new method for rapidly identifying the crystalline orientation in studying the related mechanical properties, and it is useful for flexible, stretchable, and wearable electronics.[30]

Table 4. Frequency changes (in units of cm^{-1}) under distinct strain (Pi is the ith point in Figure 3h). The angle θ was calculated according to the frequency changes set.

Points	$\Delta\omega_1(A_g^1)$	$\Delta\omega_1(B_{2g})$	$\Delta\omega_3(A_g^2)$	Angle θ [°][a]
(P1, P4)	−0.933	−4.56	−2.09	23.8
(P1, P5)	−1.456	−5.52	−2.273	31.7
(P3, P4)	−0.343	−1.644	−0.346	31.5

[a]Determined with Equations (13) and (16) by ($\Delta\omega_1$, $\Delta\omega_2$, $\Delta\omega_3$).

Another issue is the sign of θ, which is positive or negative. Three characteristic Raman bands of the BP samples can be observed under the typical backscattering geometry, with the measured frequencies denoted as ω_1, ω_2, and ω_3. After applying in-plane arbitrary uniaxial strain, the frequencies move to ω_1', ω_2', and ω_3'. The changes of frequencies are $\Delta\omega_1 = \omega_1' - \omega_1$, $\Delta\omega_2 = \omega_2' - \omega_2$, and $\Delta\omega_3 = \omega_3' - \omega_3$. According to our method, the strain angle θ can be determined by the frequency changes under strain $\theta = f(\Delta\omega_1\,\Delta\omega_2\,\Delta\omega_3)$ using Equations (13) and (16). However, because $\cos(-\theta) = \cos\theta$, the sign of θ is undetermined in this approach. As shown in **Figure 4**, the strain axis may be located in the clockwise (negative θ) or counterclockwise (positive θ) direction relative to the ZZ axis of the BP sample. To determine the sign of θ, which is necessary for complete determination of the crystalline orientation, we propose to rotate the strain axis 45° counterclockwise with respect to the previous strain direction and make an extra measurement. Denoting the resulting Raman shifts as ω_1'', ω_2'', and ω_3'', we can calculate $\Delta\omega_1' = \omega_1'' - \omega_1$, $\Delta\omega_2' = \omega_2'' - \omega_2$, and $\Delta\omega_3' = \omega_3'' - \omega_3$, and obtain a new angle: $\theta' = f(\Delta\omega_1'\,\Delta\omega_2'\,\Delta\omega_3')$. If $\theta' > 45°$, the original θ is positive, and if $\theta' < 45°$, θ is negative. Based on this scheme, the crystalline axes of the BP structures can be determined completely. Determination of the orientation by our strain-based model only needs three sets of Raman shifts $[(\omega_1, \omega_2, \omega_3), (\omega_1', \omega_2', \omega_3'), \text{and } (\omega_1'', \omega_2'', \omega_3'')]$, in principle, corresponding to recording three Raman spectra.

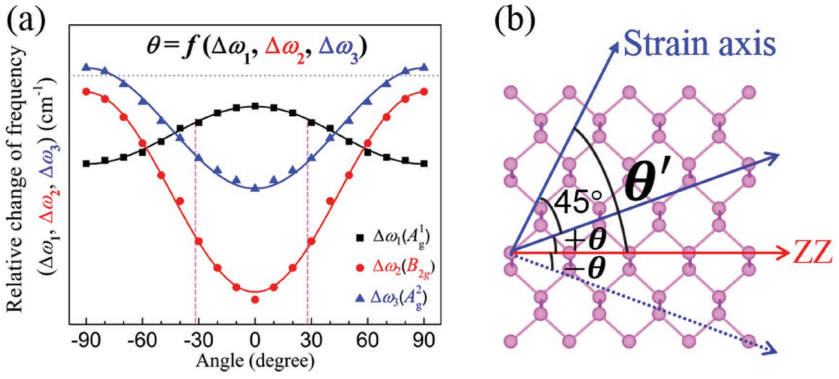

Figure 4. Direction of the strain relative to the ZZ axis of BP. a) Changes of the three characteristic Raman modes as a function of strain angle. b) Relative angle of the strain axis with respect to the ZZ direction of the monolayer BP lattice. The blue solid arrow with a positive angle mean strain in the counterclockwise direction, and the dotted blue arrow with a negative angle means strain in the clockwise direction.

3. Conclusion

An effective method to identify the crystalline orientation of BP samples by the strain-induced Raman shifts is developed, and the method is shown to be suitable for different experimental conditions. Evolution of the Raman spectra with gradually increased strain along the ZZ, 30°, and AC directions was experimentally investigated, and the angles determined with the proposed method are in good agreement with those from the polarized Raman method. Different excitation wavelengths, sample thicknesses, and substrates, as well as different experimental conditions have little influence on determination of the crystalline orientation for stretchable BP flakes, further proving the validity of the method. Furthermore, we developed an approach to estimate the efficiency of the applied strain for different BP samples. It suggests that only 20–40% of the strain is effectively transferred to BP flake from the PET substrate for the spread BP@PET setup. This is instructive and meaningful for investigating the strain related properties of BP, as well as for investigating other layered materials. Our method provides a better understanding of the strain effect on the Raman shifts of BP, and its generalization to other 2D crystals is straightforward.

4. Experimental Section

Calculation Methods: All of the calculations were carried out by DFT using the QUANTUM ESPRESSO package.[31] The generalized gradient approximation with the Perdew–Burke–Ernzerhof (PBE) method was used to deal with the exchange correlation functional.[32] The van der Waals (vdW) interactions were considered by the DFT-D2 approach of Grimme (denoted as PBE+D2),[33] vdW density functional methods optB88-vdW (denoted as PBE+B88), and optB86b-vdW (denoted as PBE+B86b)[34] in the calculations of lattice parameters and optical phonon frequencies. See the Supporting Information for detailed results and analysis. For monolayer BP, at least 10 Å gaps between layers were set to eliminate the possible interactions. The Brillouin zones were sampled on an $8 \times 8 \times 10$ Monkhorst-Pack grid[35] for bulk BP and a $14 \times 1 \times 10$ grid for monolayer BP. The structures were relaxed until all components of forces were less than 0.001 Ry $Bohr^{-1}$. The plane wave cutoff was set to 80 Ry for wave functions and 320 Ry for charge density within a norm-conserving pseudopotential. According to the analysis and comparison (see the Supporting Information), the PBE functional was selected to calculate the Raman shifts under strain with a scaling factor of 1.04.

Fabrication and Characterization of Exfoliated BP Flakes: The stretchable BP thin flakes used in this work were mechanically exfoliated from bulk BP crystals (Smart element) onto a flexible PET substrate using Scotch tape. The uniaxial strain was applied on the PET substrate with the BP sample through a home-built setup (see Figure S8 in the Supporting Information for more details). An Olympus (BX51) optical microscope with a normal white light source (tungsten halogen lamp, excitation range from 350 to 850 nm) was used for the optical images and contrast measurements. The strained Raman measurements were performed after determining the crystalline orientation. All of the Raman spectroscopy measurements were performed with a JY Horiba HR800 Raman system with the 514.5 nm (2.41 eV) line from an Ar^+ laser. The intensity of the laser was less than 100 μW to avoid damaging the BP samples.

Supporting Information

Supporting Information is available from the Wiley Online Library or from the author.

Acknowledgements

This work was supported by the National Natural Science Foundation of China (Grant Nos. 21373015, 21233001, and 21573004), the Ministry of Science and Technology (Grant Nos. 2016YFA0200101, 2016YFA0200104, and 2015CB932400), and the China Postdoctoral Science Foundation (Grant no. 2015M580010).

Conflict of Interest

The authors declare no conflict of interest.

[1] H. O. Churchill, P. Jarillo-Herrero, *Nat. Nanotechnol.* **2014**, *9*, 330.
[2] P. W. Bridgman, *J. Am. Chem. Soc.* **1914**, *36*, 1344.
[3] J. Qiao, X. Kong, Z. X. Hu, F. Yang, W. Ji, *Nat. Commun.* **2014**, *5*, 4475.
[4] V. Tran, R. Soklaski, Y. Liang, L. Yang, *Phys. Rev. B* **2014**, *89*, 235319.
[5] A. Morita, *Appl. Phys. A* **1986**, *39*, 227.
[6] L. Li, Y. Yu, G. J. Ye, Q. Ge, X. Ou, H. Wu, D. Feng, X. H. Chen, Y. Zhang, *Nat. Nanotechnol.* **2014**, *9*, 372.
[7] A. Castellanos-Gomez, L. Vicarelli, E. Prada, J. O. Island, K. L. Narasimha-Acharya, S. I. Blanter, D. J. Groenendijk, M. Buscema, G. A. Steele, J. V. Alvarez, H. W. Zandbergen, J. J. Palacios, H. S. J. van der Zant, *2D Mater.* **2014**, *1*, 025001.
[8] J. Qiao, X. Kong, Z. X. Hu, F. Yang, W. Ji, *Nat. Commun.* **2014**, *5*, 5475.
[9] X. Ling, H. Wang, S. Huang, F. Xia, M. S. Dresselhaus, *Proc. Natl. Acad. Sci. USA* **2015**, *112*, 4523.
[10] J. W. Jiang, H. S. Park, *Nat. Commun.* **2014**, *5*, 4727.
[11] F. Xia, H. Wang, Y. Jia, *Nat. Commun.* **2014**, *5*, 5458.
[12] H. Lang, S. Zhang, Z. Liu, *Phys. Rev. B* **2016**, *94*, 235306.
[13] X. Ling, S. Huang, E. H. Hasdeo, L. Liang, W. M. Parkin, Y. Tatsumi, A. R. Nugraha, A. A. Puretzky, P. M. Das, B. G. Sumpter, D. B. Geohegan, J. Kong, R. Saito, M. Drndic, V. Meunier, M. S. Dresselhaus, *Nano Lett.* **2016**, *16*, 2260.
[14] J. W. Jiang, *Nanotechnology* **2015**, *26*, 055701.
[15] A. C. Ferrari, D. M. Basko, *Nat. Nanotechnol.* **2013**, *8*, 235.
[16] Y. Feng, W. Zhou, Y. Wang, J. Zhou, E. Liu, Y. Fu, Z. Ni, X. Wu, H. Yuan, F. Miao, B. Wang, X. Wan, D. Xing, *Phys. Rev. B* **2015**, *92*, 054110.
[17] J. Wang, S. Zhang, J. Zhou, R. Liu, R. Du, H. Xu, Z. Liu, J. Zhang, Z. Liu, *Phys. Chem. Chem. Phys.* **2014**, *16*, 11303.
[18] J. Wu, N. Mao, L. Xie, H. Xu, J. Zhang, *Angew. Chem. Int. Ed.* **2015**, *54*, 2366.
[19] H. B. Ribeiro, M. A. Pimenta, C. J. de Matos, R. L. Moreira, A. S. Rodin, J. D. Zapata, E. A. de Souza, A. H. Castro Neto, *ACS Nano* **2015**, *9*, 4270.

[20] W. Lu, X. Ma, Z. Fei, J. Zhou, Z. Zhang, C. Jin, Z. Zhang, *Appl. Phys. Lett.* **2015**, *107*, 021906.
[21] J. Kim, J. U. Lee, J. Lee, H. J. Park, Z. Lee, C. Lee, H. Cheong, *Nanoscale* **2015**, *7*, 18708.
[22] N. N. Mao, J. X. Wu, B. W. Han, J. J. Lin, L. M. Tong, J. Zhang, *Small* **2016**, *12*, 2627.
[23] X. Ling, L. Liang, S. Huang, A. A. Puretzky, D. B. Geohegan, B. G. Sumpter, J. Kong, V. Meunier, M. S. Dresselhaus, *Nano Lett.* **2015**, *15*, 4080.
[24] Y. Wang, C. Cong, R. Fei, W. Yang, Y. Chen, B. Cao, L. Yang, T. Yu, *Nano Res.* **2015**, *8*, 3944.
[25] Y. Li, Z. Hu, S. Lin, S. K. Lai, W. Ji, S. P. Lau, *Adv. Funct. Mater.* **2017**, *27*, 1600986.
[26] M. Huang, H. Yan, C. Chen, D. Song, T. F. Heinz, J. Hone, *Proc. Natl. Acad. Sci. USA* **2009**, *106*, 7304.
[27] C. Rice, R. J. Young, R. Zan, U. Bangert, D. Wolverson, T. Georgiou, R. Jalil, K. S. Novoselov, *Phys. Rev. B* **2013**, *87*, 081307.
[28] S. Q. Zhang, J. Y. Wang, Z. Z. Li, R. Q. Zhao, L. M. Tong, Z. F. Liu, J. Zhang, Z. R. Liu, *J. Phys. Chem. C* **2016**, *120*, 10605.
[29] R. Fei, L. Yang, *Appl. Phys. Lett.* **2014**, *105*, 083120.
[30] K. Nomura, H. Ohta, A. Takagi, T. Kamiya, M. Hirano, H. Hosono, *Nature* **2004**, *432*, 488.
[31] P. Giannozzi, *J. Phys.: Condens. Matter* **2009**, *21*, 395502.
[32] J. P. Perdew, K. Burke, M. Ernzerhof, *Phys. Rev. Lett.* **1996**, *77*, 3865.
[33] S. Grimme, *J. Comput. Chem.* **2006**, *27*, 1787.
[34] M. Dion, H. Rydberg, E. Schroder, D. C. Langreth, B. I. Lundqvist, *Phys. Rev. Lett.* **2004**, *92*, 246401.
[35] H. J. Monkhorst, J. D. Pack, *Phys. Rev. B* **1976**, *13*, 5188.

Received: February 10, 2017
Revised: April 27, 2017
Published online: June 9, 2017

